Journal of Structural Geology, Vol. 7, No. 5, pp. 591 to 603, 1985
Printed in Great Britain

0191-8141/85 $03.00 + 0.00

Early fracture evolution within the Eye–Dashwa Lakes pluton, Atikokan, Ontario, Canada

JOHN MCEWEN and ELIZABETH HILLARY

Applied Geoscience Branch, Atomic Energy of Canada Ltd, Whiteshell Nuclear Research Establishment, Pinawa, Manitoba ROE 1LO, Canada

(*Received* 5 *December* 1983; *accepted in revised form* 21 *November* 1984)

Abstract—The fracture history of part of the Eye–Dashwa Lakes pluton near Atikokan, Ontario was investigated from drill core and surface fracture data. The earliest fractures contain aplite and compose less than 5% of the population. They developed during the initial stages of plutonic cooling and contraction, in response to local magma-related pressures. Internal pressures decreased as the pluton cooled. Subsequent fractures, comprising more than 90% of the population, formed soon afterwards under the influence of a regional subhorizontal NW–SE compression. Statistical analysis and field evidence indicate that subhorizontal and moderately dipping dip–slip fractures are filled mainly with epidote. These were followed by formation of steeply dipping to subvertical strike–slip fractures that are filled mainly with chlorite. The resulting fracture framework was well established by the end of the Archaean. Minor stress changes since then have rejuvenated the old fracture zones rather than creating new zones.

INTRODUCTION

GRANITIC ROCKS are being considered as potential hosts for long-term underground disposal of nuclear fuel wastes. The most probable way that such materials in underground excavations may return to the biosphere while still toxic is by movement in aqueous solution along fracture pathways. Therefore knowledge of fracture development with time and of fracture distribution in a rock mass is of paramount importance.

The Eye–Dashwa Lakes pluton near Atikokan, northwestern Ontario, is the subject of ongoing multidisciplinary studies to provide more information about the physical characteristics of granitic rocks (Stone 1981). To investigate the development of fracturing in the area, the pluton and surrounding gneisses were mapped in detail (Brown *et al.* 1980, Stone 1980). An area of outcrop, termed the grid area (Fig. 1), near the southeast edge of the pluton was cleared of overburden for detailed fracture mapping (Stone 1980). For subsurface investigations, oriented core was retrieved from five boreholes (ATK-1 to ATK-5) that were drilled beneath the grid area to a depth of over one kilometre (Fig. 2) (Dugal *et al.* 1981). The oriented subsurface data were plotted on equal-area lower-hemisphere stereonets (prepared from a computer routine called STEREO, available from the Computer Science Center of Energy Mines and Resources, Ottawa). These data were subjected to multiple regression analysis, to (1) determine the statistically significant fracture orientations that occur at the grid area, (2) illustrate the development of the three-dimensional fracture framework with time and (3) show the history of the development of the significant fracture orientations at the grid area in relation to stress fields resulting from pluton cooling conditions and regional deformation.

GENERAL GEOLOGY

The Eye–Dashwa Lakes pluton is a northwest trending elliptical body of medium to coarse grained hornblende–biotite granite of Archaean age, which intrudes tonalite–granodiorite gneisses of the Wabigoon Volcanic Belt in the Superior Province (Fig. 1). Large gneissic inclusions occur within the pluton. Secondary foliations, lineations, folds and evidence of penetrative ductile deformation are rare in the pluton, but are prevalent within the surrounding gneissic country rock and enclosed gneissic fragments. Compositional zoning and a weak fabric defined by distribution and alignment of quartz, feldspar and hornblende grains characterize the rim of the pluton (Brown *et al.* 1980).

The fractures within the Eye–Dashwa pluton can be subdivided on the basis of filling materials (Stone & Kamineni 1982). The oldest fractures in the grid area contain aplite, which is similar in composition to granite from the pluton interior and was probably emplaced before the interior solidified. Subsequent fractures may contain one or more of the following materials, listed in approximate chronological order of deposition: epidote, chlorite, haematite, gypsum, calcite, goethite and clay (Kamineni & Stone in press). The similarity in composition between some of the fracture filling materials and alteration products of the rock matrix indicates that the fillings are probably derived from adjacent wall rocks (Kamineni & Dugal 1982).

METHODS OF STUDY

Limitations of borehole data

There are two major limitations to the analysis of fractures measured in drill cores. First, because

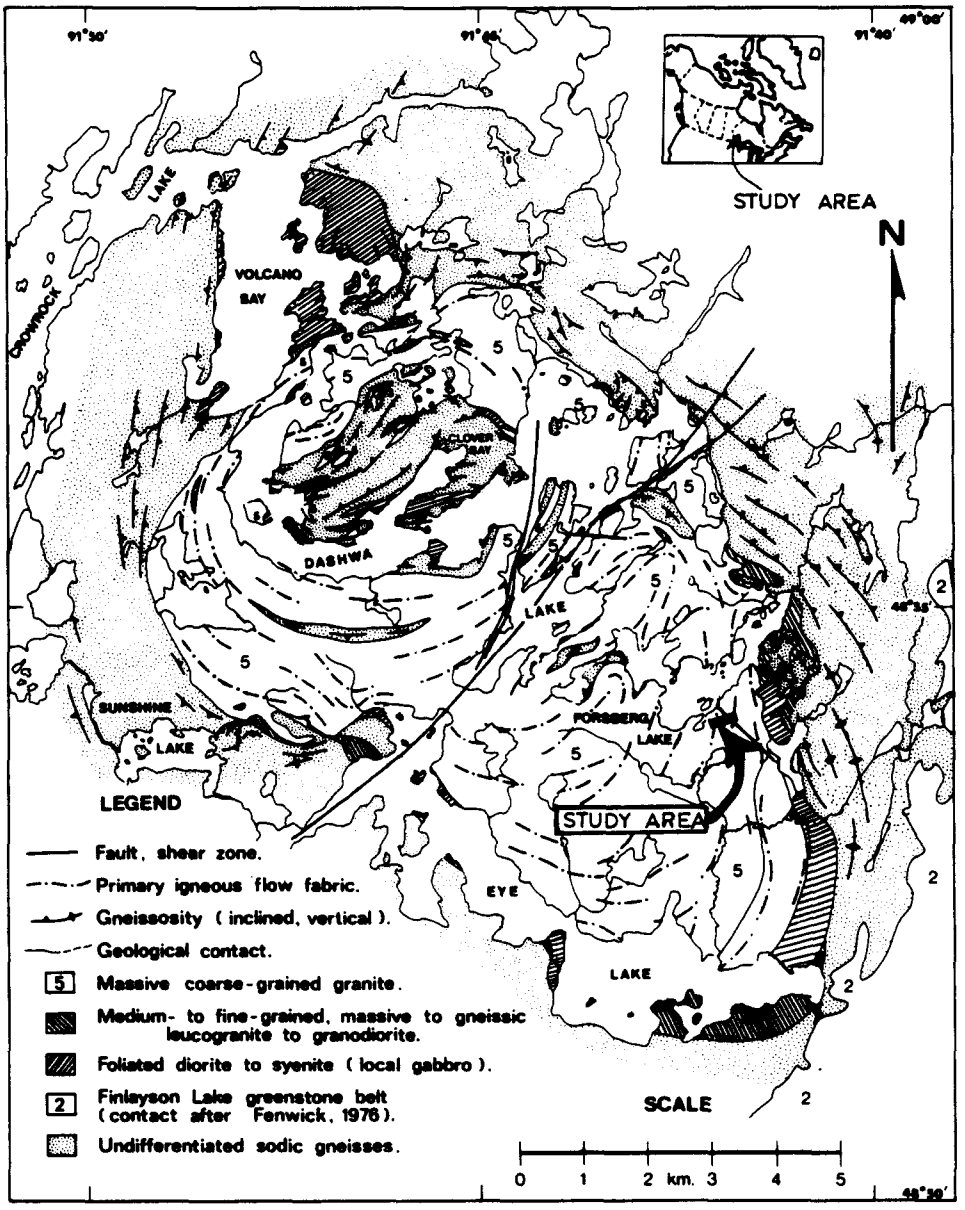

Fig. 1. General geology of the Eye–Dashwa Lakes pluton (after Brown *et al.* 1980) and grid area location.

boreholes are essentially one-dimensional features, they intersect fractures that trend at high angles to the borehole much more frequently than fractures trending at smaller angles. Therefore a subvertical borehole will intersect numerous subhorizontal fractures, but subvertical fractures that dip subparallel to the plunge of the borehole are much less likely to be intersected (Terzaghi 1965). This strong directional bias is minimized by assigning a 'Terzaghi' compensation factor to each fracture for frequency counts, so that a fracture perpendicular to the borehole is counted only once, but a fracture at angle α to the borehole is counted ($1/\sin \alpha$) times, to an arbitrary maximum of 12.

The second limitation in using borehole data is that the borehole intersects a very small part of an individual fracture, which is not necessarily a planar feature, so that the orientation measured from the core is at best approximate. Therefore the scatter in the orientation data is expected to be higher than in surface data, where the measured orientation tends to be more representative of the feature. The overlap caused by scatter from adjoining data sets, a significant factor that must be considered in any statistical analysis, is doubly important in subsurface data. In this paper, five large fracture-orientation groups from the raw borehole data are split on the basis of orientation into a total of eleven subgroups or sets to minimize the problem of possible overlapping data populations in subsequent correlation data analysis.

In addition to these major considerations, the data from the Atikokan area have certain specific limitations, which are the weakest links in this study. Firstly, the subsurface data come from a volume of rock less than one cubic kilometre, while we are attempting to relate our findings to regional structural environments. Secondly, the slip-sense data come from a few surface

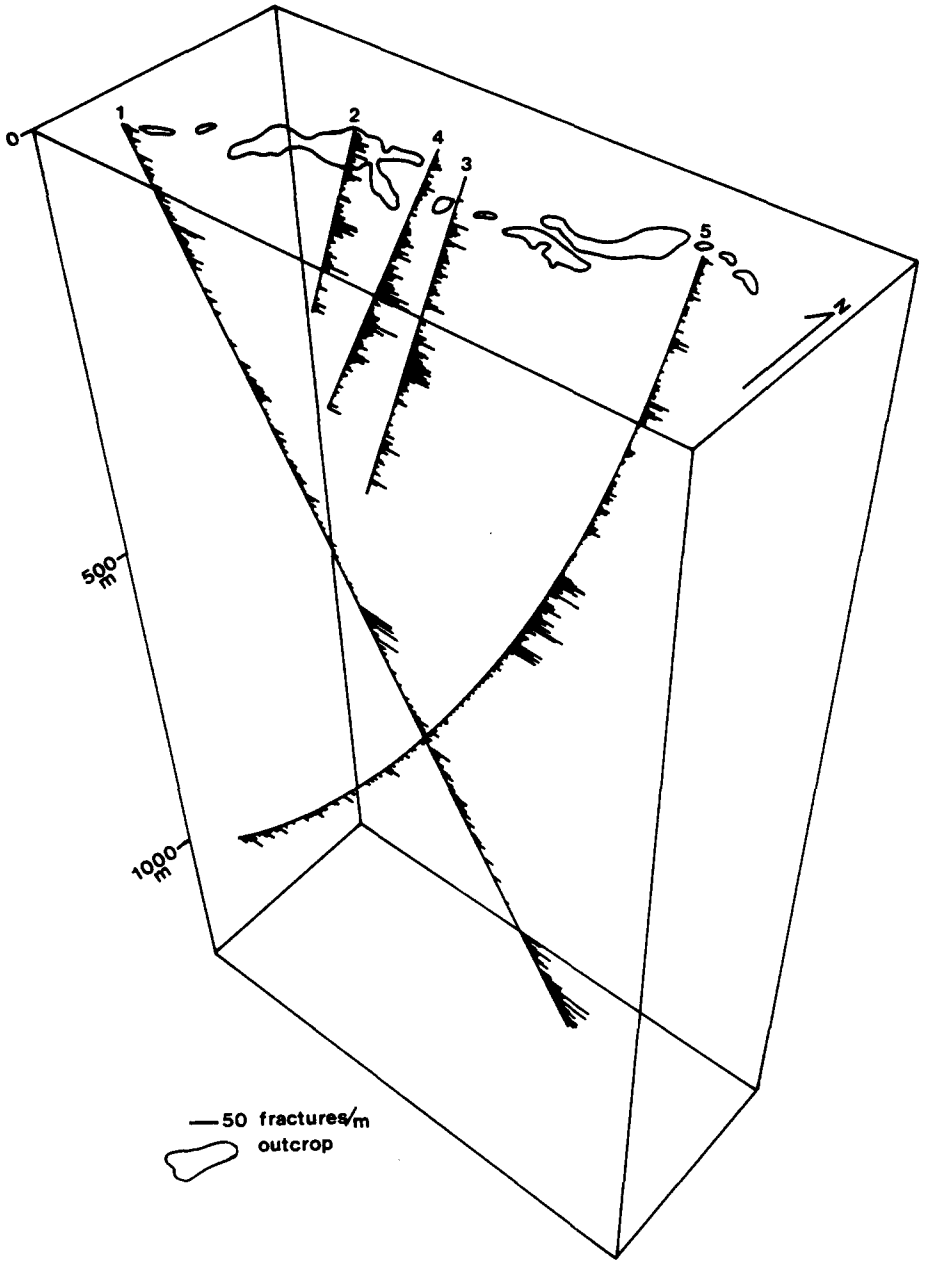

Fig. 2. Three-dimensional diagram of grid site (location shown in Fig. 1) showing areas of cleared outcrop that provided data for surface fracture studies, and array of five boreholes ATK-1 to ATK-5; fracture frequency bar charts are plotted along the boreholes.

observations rather than from the subsurface, and therefore we must assume that the surface fracture history is directly correlatable with the subsurface.

Fracture data

Orientation of aplite dykes. In outcrop, cross-cutting relationships were used to establish at least two main ages of aplite dyke formation (Stone & Kamineni 1982). A stereonet of poles to aplite dykes at the surface of the grid area ('S' in Fig. 3) indicates an early family of dykes with poles well scattered in the north and west sections of the plot and a later family clustered with a mean trend and plunge of 173°/39°. A. Brown (pers. comm. 1983) reports a separate small grouping of dykes subparallel to the local primary foliation (Fig. 3).

The subsurface rock mass at the grid area is subdivided according to boreholes: equal-area stereonets of poles to aplite dykes for each subdivision are also shown in Fig. 3. No information is available concerning the relative ages of subsurface dykes, but in each borehole the poles tend to plot along a great circle on the equal-area net and thus define a girdle.

The correlation between surface and subsurface dyke populations (Fig. 3) is relatively poor, possibly because surface mapping preferentially records steeply dipping dykes, and because the Terzaghi weighting factor is not as effective at removing orientational biases in the small dyke populations available from the subsurface. However, surface mapping indicates that poles to early aplite dykes tend to occur in the NW quadrant of the stereonet, while poles to later dykes are clustered in the SE quad-

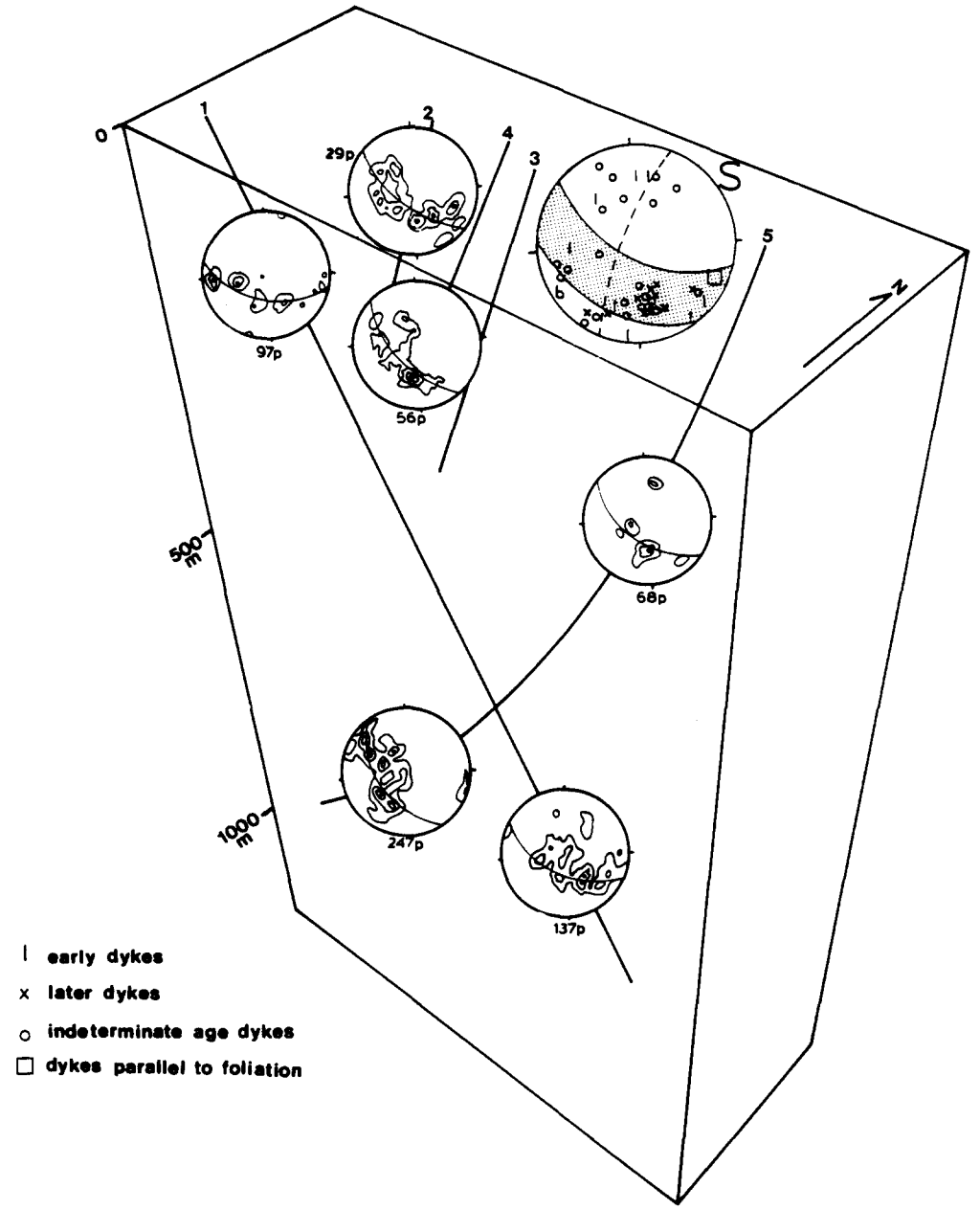

Fig. 3. Equal-area stereonets of poles to aplite dyke distributions on surface and in subsurface. Single line dashed girdle approximates local foliation, and broad shaded girdle on 'S' incorporates all girdles from subsurface nets (girdles fitted by hand).

rant. This suggests that the girdles in the subsurface dyke populations (Fig. 3) trace a younging of poles to dykes from the western to the southeastern section of each stereonet.

Orientation of subsequent fracturing. About 13,000 fractures were measured in 3000 m of oriented core recovered from boreholes ATK-1 to ATK-5 (Fig. 2) (Dugal *et al.* 1981). The NQ-3 size (76 mm) holes were drilled using a triple core barrel, so core retrieval was consistently almost 100%. To simplify this large amount of data for structural analysis, the Kamb technique (Kamb 1959) of contouring stereonet data was used. Kamb calculated the radius r of the counting circle for stereonets of 10 cm radius to be $r = (30\,(N + 9) - \frac{1}{2})$, for N data points. This produces contours which are related to the standard deviation σ of the sample, so that $\sigma = (NA(1 - A))^{\frac{1}{2}}$, where A is the area of the counting circle expressed as a fraction of the net area. In this way, five statistically significant fracture orientation groups, A–E (Figs. 4a & b), were defined by the 4σ Kamb contours. Using variable counting cell sizes, contoured stereonets of poles to all fractures within the 2σ Kamb contour were analysed visually to distinguish subgroups, or sets, within each of these five major orientation groups (Figs. 4c–e).

Where sets overlapped and were not visually distinct, the following methods were adopted for set distinction.

(1) Assume that all the fracture data conform to a spherical normal distribution.

(2) Isolate the region on the stereonet containing the data being investigated.

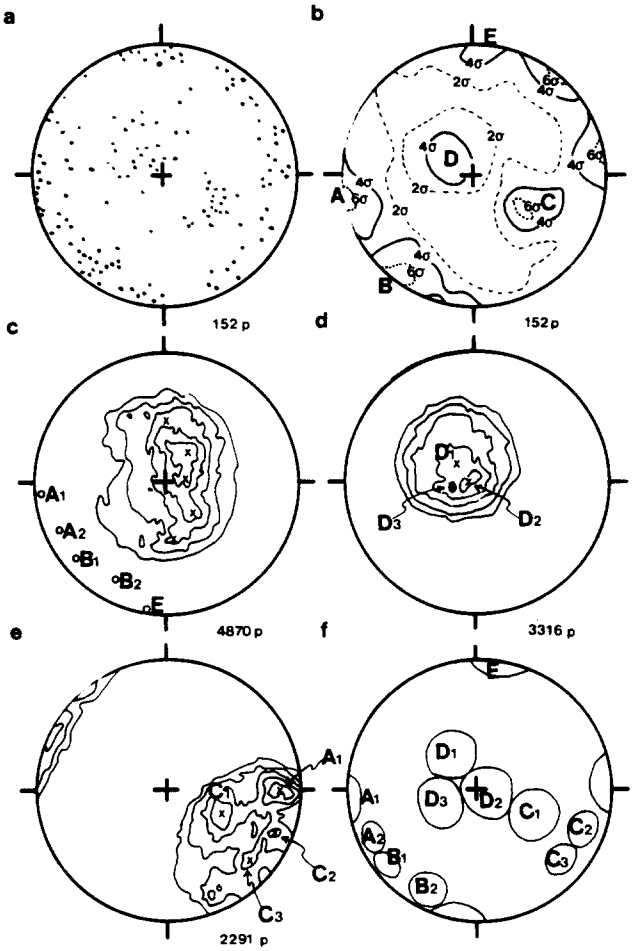

Fig. 4. Derivation of sets used in statistical correlations. All data are 'Terzaghi' weighted, and plotted on equal-area stereonets. (a) Mean orientation of subsurface data clusters of fractures grouped in 100 m intervals. Each point represents the mean of approximately 50 fracture orientations. (b) Kamb (1959) contour plot of (a); radius = 2.38 cm, standard deviation = 2.83. (c) Discrimination between fracture sets A_1, A_2, B_1, B_2 and E. In this case discrimination was simplified when the data were rotated to the centre of the stereonet. O and X are the true and rotated positions respectively of set peak orientations. (d) Discrimination between fracture sets D_1, D_2 and D_3. (e) Discrimination between fracture sets C_1, C_2, C_3 and A_1. (f) Eleven non-overlapping fracture sets derived from subsurface fracture population, to be used in regression analysis.

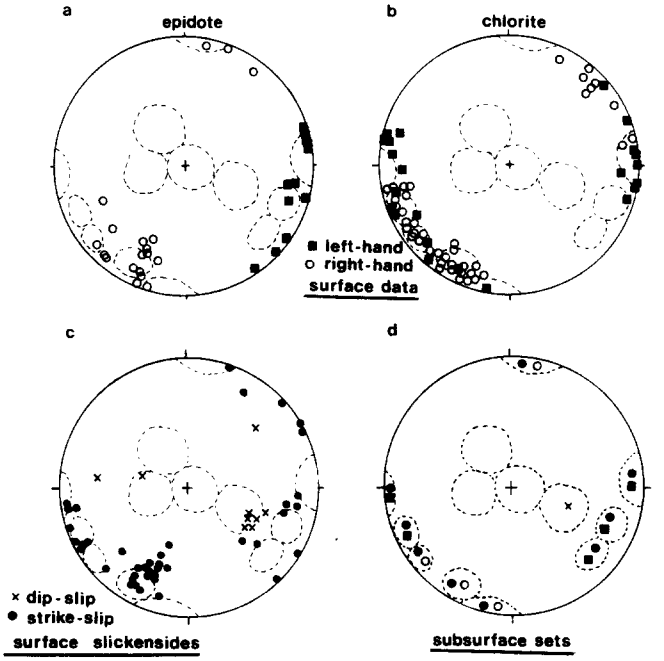

Fig. 5. Summary of surface information concerning sense of displacement along epidote and chlorite filled faults in the grid area. Surface data in (a)–(c) are used to assign senses of displacement to subsurface fracture sets in (d). Data in (a) and (b) from Stone & Kamineni (1982); data in (c) from Stone, pers. comm. (1982).

(3) Estimate the concentration parameter for each of the suspected sets, employing the method outlined by Ramsden & Cruden (1979).

(4) Generate numerous random samples from a spherical normal distribution with the estimated concentration parameter, using an algorithm from Stauffer (1966). Determine the range in sample size from the known number of points within the isolated region.

(5) Compare the peak density estimates for each suspected set with the value (or mean value, for numerous iterations) of peak density obtained from the generated samples, using the counting circle sizes used in concentration parameter estimation. An estimate of the number of members in each suspected set is obtained when these two values are approximately equal.

(6) Determine the length of the vector resultant for each suspected set (McFadden 1980).

(7) Apply the *F*-statistic test for comparison of the two mean directions for each pair of suspected sets (McFadden & Lowes 1981) to determine if the sets are statistically distinct. Figure 4(f) is a stereonet of the non-overlapping zones of influence for each of the eleven major fracture sets. Mean orientations were derived by vectorial summation and the boundaries for each set were chosen by a combination of contour value and visual inspection.

Some surface fracture sets are characterized by dip–slip or strike–slip movement (Fig. 5). Unfortunately, slip-sense data were not collected from the cores, and therefore the available surface data were used. These data are used to assign senses of movement to the subsurface sets with the same orientation. Slickenside pitch measurements on surface fractures indicate that moderately dipping, NE-striking fractures in the grid area (set C1) tend to show dip-slip movement, while steeply dipping fractures tend to be strike–slip (Fig. 5c) (Stone, pers comm. 1982).

Regression analysis of subsurface fracture orientations and filling data

To examine the occurrence of various sets together in fracture zones, and the preference for various filling materials in each set, fracture zones or samples defined by high fracture density were selected from the five boreholes. Fractures not occurring in one of the eleven orientation sets (Fig. 4f) were excluded from further analysis.

A Kamb contoured equal-area stereonet of poles to fractures occurring within these zones compares favourably with a stereonet representing the entire data base (Fig. 4b). The number of fractures in each sample was

Table 1. Correlation matrices of fracture sets. (a) Fractures containing all filling types (sample = 81 fracture zones). (b) Fractures containing epidote (sample = 56 fracture zones). (c) Fractures containing chlorite (sample = 77 fracture zones). (d) Fractures containing haematite (sample = 80 fracture zones)

	A1	A2	B1	B2	C1	C2	C3	D1	D2	D3	E
(a)	Fractures containing all filling types										
A1	1.0										
A2	−0.02	1.0									
B1	0.04	0.14	1.0								
B2	−0.02	0.12	0.18	1.0							
C1	0.01	−0.19	−0.18	−0.04	1.0						
C2	0.15	0.04	−0.06	0.03	−0.09	1.0					
C3	−0.05	0.12	0.17	0.18	−0.06	0.17	1.0				
D1	0.10	−0.10	*−0.25*	0.11	**0.35**	−0.01	−0.12	1.0			
D2	0.01	0.05	−0.07	0.07	**0.26**	0.14	−0.13	**0.29**	1.0		
D3	0.02	−0.14	*−0.23*	−0.11	−0.08	−0.05	−0.07	0.12	0.12	1.0	
E	0.13	−0.03	−0.05	*0.27*	−0.03	**0.25**	0.10	−0.11	−0.07	−0.01	1.0
(b)	Fractures containing epidote										
A1	1.0										
A2	**0.25**	1.0									
B1	**0.36**	**0.39**	1.0								
B2	**0.24**	**0.65**	**0.27**	1.0							
C1	−0.05	−0.09	−0.15	−0.05	1.0						
C2	*0.48*	*0.26*	0.16	*0.26*	−0.09	1.0					
C3	0.08	−0.01	−0.05	−0.01	−0.05	**0.73**	1.0				
D1	−0.14	−0.07	−0.18	−0.16	**0.38**	−0.11	−0.08	1.0			
D2	−0.09	−0.12	−0.17	−0.07	**0.49**	−0.05	−0.06	**0.43**	1.0		
D3	0.10	−0.05	−0.12	−0.11	0.09	−0.07	0.00	**0.27**	**0.28**	1.0	
E	0.19	*0.40*	0.09	*0.64*	0.07	0.14	−0.05	−0.07	*0.22*	0.00	1.0
(c)	Fractures containing chlorite										
A1	1.0										
A2	0.02	1.0									
B1	**0.30**	**0.35**	1.0								
B2	0.04	0.05	**0.25**	1.0							
C1	0.10	−0.10	−0.11	0.05	1.0						
C2	*0.20*	0.11	0.09	−0.08	0.03	1.0					
C3	0.18	0.11	*0.25*	0.11	0.05	**0.54**	1.0				
D1	*0.28*	−0.04	−0.10	−0.01	0.02	−0.03	0.04	1.0			
D2	−0.09	*0.27*	0.09	0.04	0.13	0.00	−0.10	**0.24**	1.0		
D3	0.10	−0.07	−0.10	−0.06	0.14	0.00	−0.04	0.11	0.04	1.0	
E	−0.08	0.11	0.00	*0.36*	0.06	0.18	0.04	0.04	0.00	−0.02	1.0
(d)	Fractures containing haematite										
A1	1.0										
A2	−0.11	1.0									
B1	0.06	**0.37**	1.0								
B2	−0.02	−0.06	**0.23**	1.0							
C1	*0.25*	−0.11	−0.14	−0.09	1.0						
C2	0.01	0.11	0.04	−0.08	−0.04	1.0					
C3	−0.10	0.09	*0.21*	−0.09	−0.09	**0.42**	1.0				
D1	0.18	0.05	−0.10	−0.04	**0.47**	0.06	−0.11	1.0			
D2	0.02	*0.29*	0.12	−0.06	**0.20**	0.07	−0.07	**0.20**	1.0		
D3	0.01	−0.05	−0.18	−0.07	−0.10	−0.14	*0.21*	0.07	−0.01	1.0	
E	0.11	−0.16	−0.01	−0.01	0.00	0.02	0.02	−0.11	−0.09	0.04	1.0

Bold type: Correlations discussed in text.

Italic type: good correlations not discussed because (a) classical indicators for conjugate sets (good dihedral angle, shear movement and epidote/chlorite ratios) do not suggest a relationship (e.g. D1, B1) or (b) immediate proximity of two sets indicates good correlation may be caused by overlap of populations (e.g. E, B2; A1, C2).

normalized to account for differences in sample size and density, where density is defined as Terzaghi-weighted fracture frequency per metre of borehole length. Matrices of correlation coefficients (Table 1) were constructed and multiple regression analyses (Nie *et al.* 1975) were performed on the normalized fracture frequencies of the orientation sets regardless of filling material, and on the orientation sets composed of fractures containing epidote, chlorite and haematite. The filling materials were also correlated with each other (Table 2), regardless of the orientation of their fractures. For example, the positive correlation (0.35) between the numbers of fractures in sets C1 and D1 in 81 sampled fracture zones (Table 1a) shows that the pair of sets is spatially related. This spatial correlation is probably valid even between conjugate pairs, since the fracture data gathered by the core-log survey include fractures as narrow as 0.1 mm. Therefore both conjugate pairs should be represented to some extent in the data base.

In subsequent analyses, the grouping of fracture sets into conjugate pairs is based on dihedral angles, epidote/chlorite ratios (Table 3) and senses of shear movement

Table 2. Correlation matrix of filling types (sample = 104 fracture zones)

	Epidote	Chlorite	Haematite	Calcite	Clay	Goethite	Gypsum
Epidote	1.00000						
Chlorite	−0.11137	1.00000					
Haematite	−0.10711	0.55366	1.00000				
Calcite	−0.02759	0.38225	0.48395	1.00000			
Clay	−0.16587	0.17271	0.28268	0.32645	1.00000		
Goethite	−0.11390	0.14120	0.12107	0.14928	0.57181	1.00000	
Gypsum	0.41479	−0.11740	−0.05945	−0.10544	−0.08508	−0.12098	1.00000

(Fig. 5), as well as on the correlation coefficients (Table 1). This explains why some of the high correlation coefficients were not considered sufficient evidence in themselves for conjugate pairs, in the following discussion.

Three-dimensional fracture framework

In order to plot the fracture framework in three-dimensional space, fracture data were grouped according to orientation and spatial position by a technique based on data clustering (Bailey 1975). The 'distance' between data points (fractures) in this clustering technique is determined from a combination of separation angle of fracture poles and the actual distance between fractures measured from the drill core. Fracture filling and rock alteration proportions, fracture density (fractures/metres), average fracture thickness and mean orientation were noted for each of the fracture groups or clusters. Correlation of the fracture clusters between boreholes is achieved on the basis of 3-D projection and similarity in these fracture characteristics.

RESULTS OF STUDY

Stress configuration during aplite emplacement

Because the aplite dykes were injected soon after the emplacement of the pluton (Stone & Kamineni 1982), the orientation of aplite dykes in the grid area provides information about the early stress history of that part of the pluton. Assuming that surface age relationships can be applied in the subsurface, the girdles in Fig. 3 appear to trace a younging of poles to dykes from the western to the southern sections of each equal-area net. In some of the stereonets in Fig. 3, separate small clusters of poles to steeply west-dipping dykes can be found in the ESE section of the plot, indicating that they probably formed along weakness planes subparallel to the local primary foliation.

Aplite-filled fractures exhibit little evidence of displacement or refracturing. Therefore it is likely that they formed during extension, and were subsequently sealed with aplitic material. In this interpretation the poles to the dykes are assumed to be parallel to the minimum principal compressive stress direction (σ_3), and the resulting girdles in Fig. 3 thus trace out the range of σ_3 directions during aplite dyke formation. The position of the maximum and intermediate stress directions (σ_1 and σ_2) during aplite emplacement cannot be determined from dyke orientations alone. However, due to the systematic change in σ_3 orientation, it is assumed that one of the two stress directions, say σ_a, lies on the girdle and is normal to σ_3 and therefore the other stress direction (σ_b) is the pole to the girdle.

Figure 6 was constructed from the stereonet plots of aplite dyke data shown in Fig. 3. The clusters of points labelled σ_a were plotted at 90° to major concentrations of early and late dykes (Fig. 3), and therefore represent one of the major stress directions of early and late aplite dyke concentrations, respectively. The σ_b points are the poles to the girdles. Independent fault studies (Schwerdtner *et al.* 1979, Bau 1976) reveal that the area underwent NW–SE compression during emplacement of the Eye–Dashwa Lakes pluton. Therefore the σ_a

Table 3. Density of fractures and epidote/chlorite ratio in each set (fractures m^{-1})

	Set	Trend/Plunge of Pole	Fractures metre^{-1}			
			Fractures	Epidote	Chlorite	Epidote/ Chlorite ratio
Stage 1	C1	113/51	7.9	5.2	3.5	1.5
	D1	314/72	6.2	3.2	2.8	1.1
	D2	293/86	4.8	1.8	1.7	1.1
	D3	264/73	5.9	2.6	2.5	1.0
Stage 2	C2	110/15	3.3	0.8	1.7	0.5
	C3	131/19	2.5	1.3	1.9	0.7
	E	190/01	6.1	1.9	2.6	0.7
Stage 3	A1	267/01	6.3	1.2	3.6	0.3
	A2	247/16	4.9	1.4	3.5	0.4
	B1	230/12	3.9	0.7	3.4	0.2
	B2	209/18	5.9	0.8	3.8	0.2

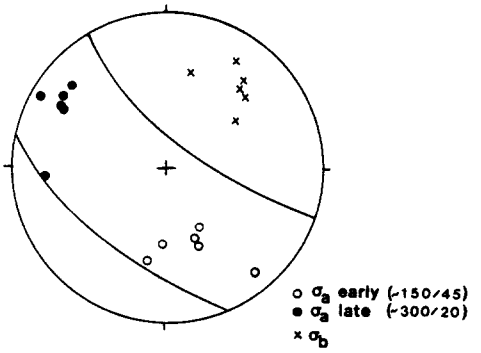

Fig. 6. Summary of stress directions which existed during intrusion of aplite dykes σ_a and σ_b are defined in the text.

stress direction is likely to be the maximum principal stress direction for the later dykes. This interpretation assumes that stress directions inside the pluton were subparallel to regional stresses during later dyke emplacement. The σ_a direction for the earlier dykes probably represents the maximum compressive stress condition inside the cooling pluton. The poles to the girdles become the σ_2 stress directions. Therefore, it is apparent that during the time of aplite dyke emplacement the principal stress direction σ_1 changed from an approximate local trend and plunge of 150°/45° to a more regionally oriented 300°/20° direction, subparallel to that suggested by Bau (1976) and Schwerdtner *et al.* (1979).

Stress configuration during subsequent fracturing

Aplite dykes represent less than 5% of the fracture population at the drill site. The remaining 95% of fractures were filled in approximate chronological order as follows: epidote, chlorite, haematite and lower temperature minerals (Stone & Kamineni 1982). The changes in the stress environment at the drill site may be determined by comparing the relative age of fillings with the orientations of the fractures they occupy.

Figure 7 shows a series of contour plots for ATK-1 and ATK-5 of poles to fractures that contain a selected filling material, although the fractures may also contain other fillings. The data were plotted for 500-m intervals to check for significant changes in orientation with depth. It is important to note from the contour plots that epidote, the earliest filling after aplite, occurs to some extent in all of the fracture sets outlined in Fig. 4(f), and that these sets occur throughout the rock mass.

Although all the fracture sets contain some epidote, the subhorizontal to moderately dipping sets D1 and C1 (Table 3, Fig. 4f) have the highest epidote filling concentrations. Tables 1(a & b) show relatively strong positive correlations between sets C1 and D1 as well as with sets D1 and D2 which also have high epidote concentrations. There are strong negative correlations between these and the remaining sets (Tables 1a & b). Correlations between the same sets weaken when the correlation matrices of orientation sets dominated by younger filling materials are examined (Tables 1c & d). Therefore, the strong positive spatial and filling correlations show that sets C1, D1, D2 and D3 comprise the earliest well developed fracture system at the grid area (Stage I).

Many of the epidote-filled fractures contain prisms of epidote, indicating strain-free growth in tension fractures, while some contain cataclastically deformed aggregates of epidote, indicating some shear movement (Stone & Kamineni 1982). It appears therefore that at least some of the fractures of the subhorizontal and moderately dipping sets initially formed in an extensional environment and were filled with epidote. Subsequent slippage along some of these pre-existing weaknesses resulted in cataclasis of the epidote. Dip–slip epidote fractures (Fig. 5a) occur in set C1. Since data describing the possible sense of movement along any fractures contained within sets D1, D2 and D3 are lacking, it cannot be stated unequivocally which of the sets forms the conjugate fractures to set C1. However, the strong positive correlation between C1 and D1 (Table 1a) suggests that D1 is the main complementary shear direction, even though D2 and D3 may have been more active at intervals during the pluton's history.

The group of sets that form the second major stage of fracturing includes C2, C3 and E. This grouping is based largely on the epidote/chlorite ratios within these sets (Table 3), correlation coefficients (Table 1) and senses of shear movement (Fig. 5). A somewhat weak positive correlation exists between sets C2 and C3 when no particular filling is considered (Table 1a) but strong positive correlations occur between them when epidote-(Table 1b) and chlorite-(Table 1c) filled fractures are considered. Assuming that both sets have right-hand shear displacement as suggested by surface observations (Fig. 5), these correlations strongly suggest that C2 and C3 belong to the same genetic fracture set. The slight difference in orientation is probably due to local differences in the response to the stress field, caused by factors such as foliation, gneissosity or other structural heterogeneities. Because set E has dextral movement and set C2–C3 has sinistral movement (Fig. 5), and they have similar epidote/chlorite ratios (Table 3) they are probably conjugate sets with respect to a subhorizontal northwest σ_1, as suggested by Stone & Kamineni (1982).

C2 is considered to be the main conjugate set to E since it is more developed than C3 (Fig. 4e) and has stronger correlations with E (Table 1). Therefore, assuming a sub-horizontal NW–SE trending σ_1 as indicated by the senses of shear movement (Fig. 5d), it is apparent that this failure complementary to E was largely directed along a pre-existing plane of weakness, namely the local primary foliation (Fig. 3).

The third stage of fracturing involved sets A1, A2, B1 and B2, which have the lowest epidote/chlorite ratios (Table 3). Sets A1 and A2 contain fractures with sinistral displacement, and are moderately and positively correlated when epidote-filled fractures are considered (Table 1b). Sets B1 and B2 contain fractures with dextral displacement and have strong positive correlations throughout Table 1. Sets A1 and A2 both have strong positive correlations with sets B1 and B2 in epidote-filled

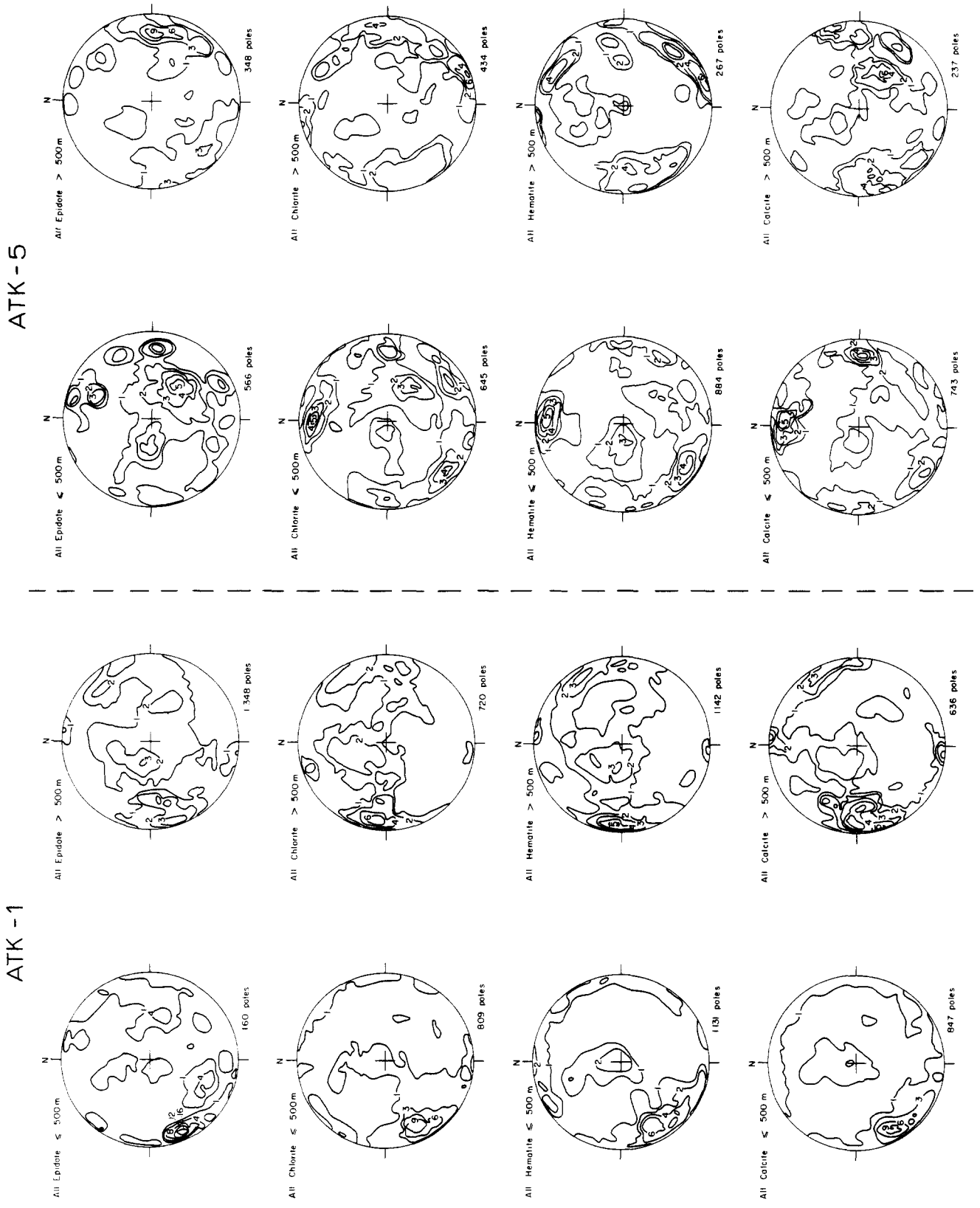

Fig. 7. Orientation of all fractures containing epidote, chlorite, haematite or calcite in boreholes ATK-1 and ATK-5. Data are 'Terzaghi' weighted, and contours are in % per 1% of the stereonet area.

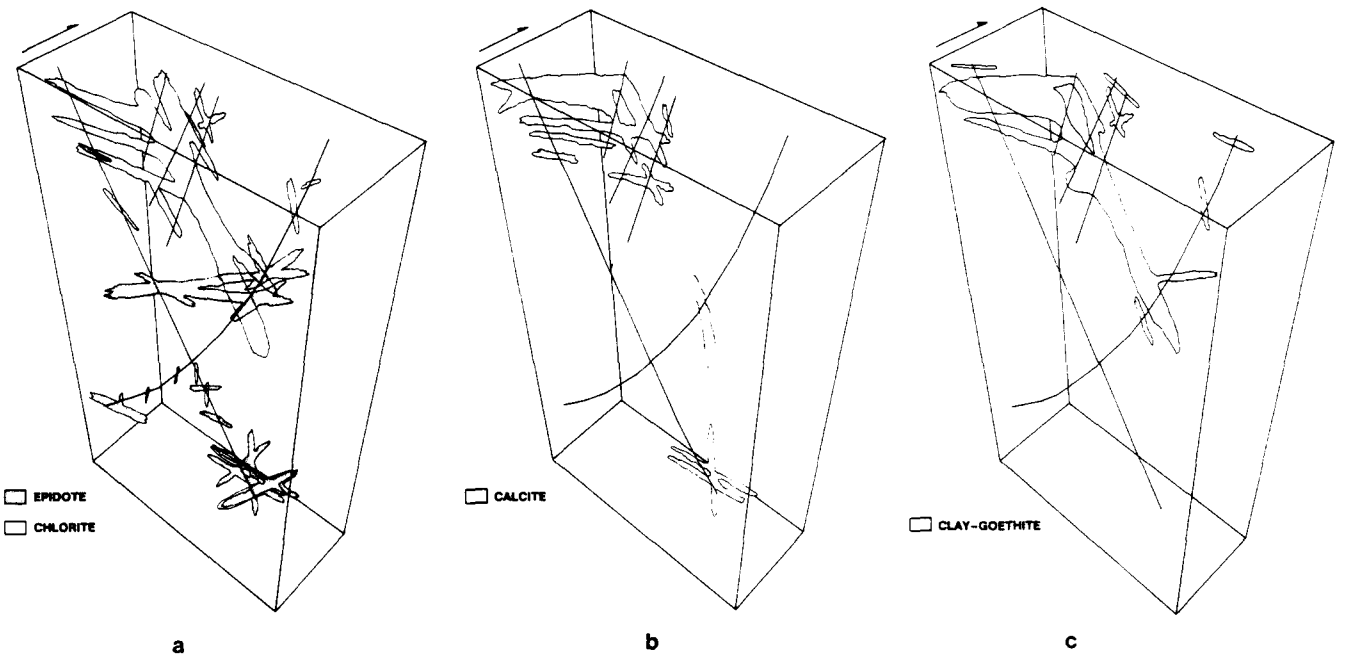

Fig. 8. Three-dimensional diagrams of the major systems rich in (a) epidote, (b) chlorite and (c) calcite, clay and geothite.

fractures (Table 1b). Therefore A1 and A2 are considered to be members of the same genetic set, and conjugate to a genetic set containing B1 and B2.

The correlation between A1–A2 and B1–B2 is strongest in epidote-filled fractures. In chlorite-filled fractures, set A1–A2 correlates best with set B1 alone (Table 1c). In haematite-filled fractures, set A2 correlates best with set B1 (Table 1d). These correlations suggest that through time, as documented by filling material, the dihedral angle between conjugate fractures decreased from 60° during the last stages of epidote formation, to less than 20° during haematite deposition, except where affected by pre-existing planes of weakness.

Correlation between filling materials

Three major conclusions can be obtained from multiple regression analysis of the occurrence of major filling materials, when orientation is not considered (Table 2). (1) Epidote correlates strongly and positively with the occurrence of gypsum, supporting the hypothesis that most of the gypsum is derived from epidote (Kamineni in press). Epidote has a low negative correlation with the remaining filling materials. (2) Chlorite, haematite, calcite and clay all have strong positive correlations, indicating that haematite, calcite and clay tend to be deposited in pre-existing chlorite-filled fractures. (3) Clay and goethite exhibit high positive correlation values, because they both tend to occur in open fractures near the surface (Fig. 8).

Three-dimensional fracture configurations

The major fracture systems rich in epidote are predominantly composed of the early sub-horizontal to moderately dipping fractures of Stage I (Fig. 8a). However, epidote is present to some degree in all fracture sets (Fig. 7), so that incipient development of the more steeply dipping systems also occurred during epidote deposition. All major fracture sets also contain chlorite-filled fractures (Fig. 7), but they are most common in steeply dipping fracture systems of Stages II and III. Figure 8(a) illustrates the fracture framework at the grid area during the Archaean, when Stage III was already well developed (Kamineni & Stone 1983, Brown *et al.* 1982).

Three-dimensional fracture configurations of the major fracture systems rich in calcite (Fig. 8b) and clay–goethite (Fig. 8c) and distribution of these filling materials within the major fracture sets (Fig. 7) indicate that the deposition of later low-temperature filling materials largely occurred in rejuvenated pre-existing fracture systems.

DISCUSSION

The sequence of fracturing described in the preceding section defines a history of the stresses that have operated at the grid area since emplacement of the pluton. Recent work by other writers, in similar structural environments, suggests that the initial fracturing probably occurred by extension within the solidifying carapace which surrounded the interior of the cooling pluton. This carapace would effectively seal off the molten interior from the country rock, causing a build-up of an internal aqueous phase during magma crystallization (Burnham & Ohmoto 1980, Knapp & Norton 1981, Hibbard 1980). Brittle extension fractures would form in the carapace when this vapour pressure exceeded lithostatic load and these fractures would subsequently fill

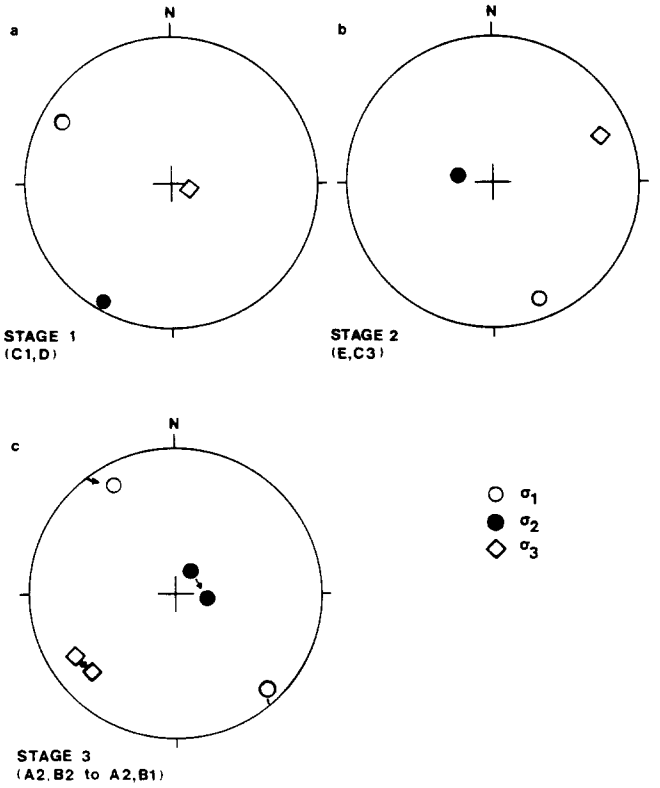

Fig. 9. Stereonet showing stress configurations during the main stages of fracturing.

with aplitic material derived from the pluton interior. The staggered clusters of poles to aplite dykes straddling the girdles (Fig. 3) could represent episodic failure of the solid carapace as the internal pressure was built up and released (Knapp & Norton 1981).

The change in orientation of aplite dykes suggests a change in the maximum compressive stress with time from a trend and plunge of 150°/45°, which may be at least partly related to early magma pressures, to 300°/20° (Fig. 6), which is subparallel to the regional NW–SE compressive environment proposed by Schwerdtner *et al.* (1979). This suggests that the earliest fractures were developed in an environment dominated by local stresses within the pluton as it was in the final stages of emplacement, while later fracturing during pluton cooling was more affected by the regional NW–SE compression into which the pluton was emplaced. The aplite dykes show little evidence of refracturing, so that subsequent fracture events were not significantly affected by pre-existing discontinuities.

The first major stage of fracturing (Stage I) after the emplacement of the aplite dykes resulted in fractures with subhorizontal to moderate dips (sets C1, D1, D2, D3; Fig. 4f). These fractures, which are predominantly filled with epidote (Table 3), were probably formed by extension due to hydraulic fracturing (Stone & Kamineni 1982) in an environment charged with abundant fluid, as indicated by the degree and amount of rock mass alteration (Kamineni & Dugal 1982). Since there is no evidence for fractures with combined shear and extension, the wide scatter in initial orientations within sets C1–D3 was probably caused by variable local stress conditions related to pluton cooling. With continued pluton cooling and increasing stability, the relatively large regional component in the stress environment led to dip–slip shearing along preferred orientations (sets C1 and probably D1) of these extension fractures. Segall & Pollard (1983) documented a similar relationship in granite where strike–slip faults nucleated on older dilatant fractures. The stress configuration required for this failure is shown in Fig. 9, and as expected, the σ_1 direction has a direction similar to that implied from the orientation of the later aplite dykes (Fig. 6).

The orientations of the steeply dipping Stage II fractures (sets E, C2), filled with epidote and chlorite, indicate that the rock mass was still subjected to a NW–SE trending σ_1, but that the subvertical principal stress direction had become the σ_2 direction (Fig. 9). The increase in strength of the subvertical principal stress could possibly reflect a change from an environment of subhorizontal compression, with some stress still related to pluton cooling and contraction (Knapp & Norton 1981), to a stress environment dominated by subhorizontal compression and lithostatic load.

Fractures within the third and last major stage are rich in chlorite filling material (Table 3). They developed under a similar stress configuration as Stage II fracturing, but exhibit a decrease in dihedral angle with time. This implies that, while fracture sets A1, A2, B1 and B2 were forming, the rock mass was subjected to a stress environment characterized by a progressively decreasing confining pressure.

The epidote/chlorite ratios (Table 3) decrease from Stage I to Stage III. Some chlorite was deposited during the later part of Stage I with epidote. The amount of epidote being deposited decreased and chlorite increased as the change in stresses gradually increased the number of steeply dipping fractures (Fig. 10). By the end of Stage II, very little epidote was being deposited, and chlorite filled the vast majority of fractures in Stage III. Because the change of filling type is time-related (Kamineni & Stone in press), it appears that the three stages of fracturing developed sequentially as the stress configuration changed. Therefore a model of simultaneous development of multiple fault systems (Reches 1978) cannot be applied to the fracture sets delineated at our study area.

Pre-existing fractures may affect the development of subsequent fracturing (Hobbs *et al.* 1976, Segal & Pollard 1983). However, weakly negative correlations between epidote and chlorite filling materials (Table 2) indicate that most epidote filled fractures were not reactivated to be filled with later chlorite. Instead, the early epidote filled fractures in general must have been sealed, and acted as part of the intact host rock mass during Stages II and III. A relatively high positive correlation between epidote and gypsum suggests that some epidote fractures were later rejuvenated and filled with gypsum (Kamineni 1983).

Chlorite, haematite, calcite, clay and goethite all show high positive correlations (Table 2), indicating that these fillings were deposited in the same fracture zones, as

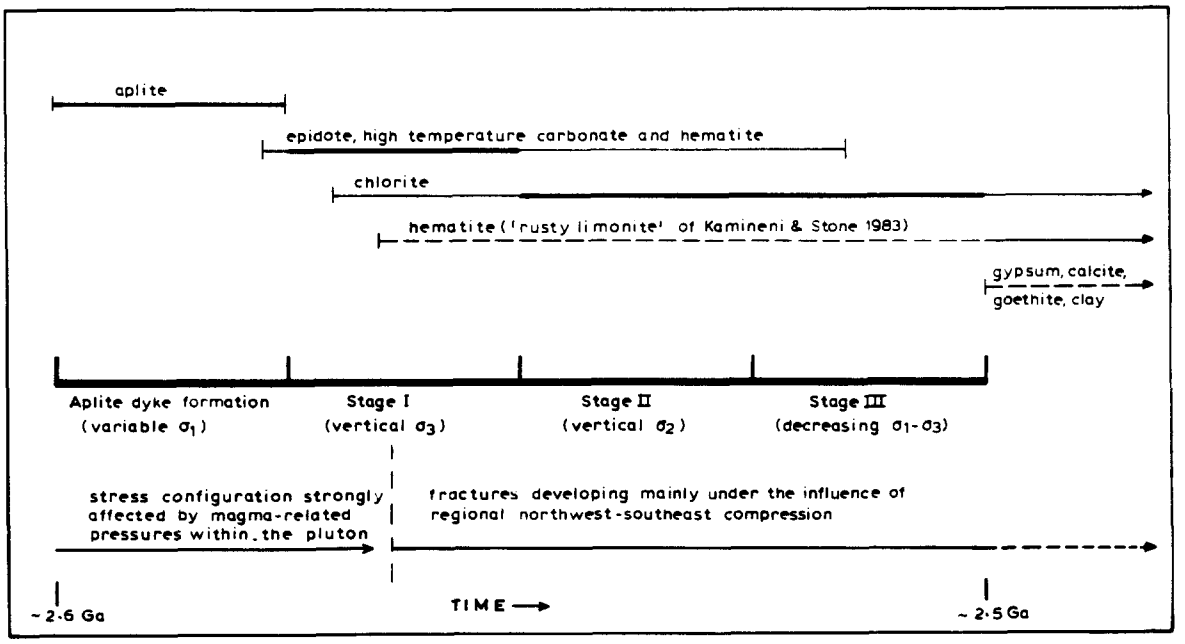

Fig. 10. Bar graph of stages of fracture formation and paragenesis of fracture fillings. Adapted from Kamineni & Stone (1983).

shown in Fig. 8. Because these fillings were deposited over a long time period (Kamineni & Stone 1983), some of the fractures in Stages II and III were rejuvenated several times. However, the more recent fillings tend to occur in only a few main fracture zones in the upper part of the drill site, and are much less abundant than the early epidote and chlorite fillings (Hillary 1982, Brown & McEwen 1982).

CONCLUSIONS

(1) During the initial stages of pluton cooling and contraction, the stress configuration in the grid area was strongly influenced by local internal magma-related pressures. The maximum principal compressive stress direction had a variable trend but probably a moderate plunge while the earliest aplite-filled tension fractures formed.

(2) As the pluton cooled the internal stresses decreased, and a regional subhorizontal NW–SE compression became the maximum principal stress, with later aplite dykes formed subparallel to it.

(3) The great majority of fractures in the grid area formed after the aplite dykes, under the influence of the regional NW–SE compression, in three stages (Fig. 11):

(a) subhorizontal and moderately dipping conjugate dip–slip fractures, indicating a subvertical minimum principal stress σ_3 (sets C1 and D);

(b) subvertical to steeply dipping strike–slip conjugate fractures, indicating that the subvertical compressive stress increased to become σ_2 (sets C2 and E);

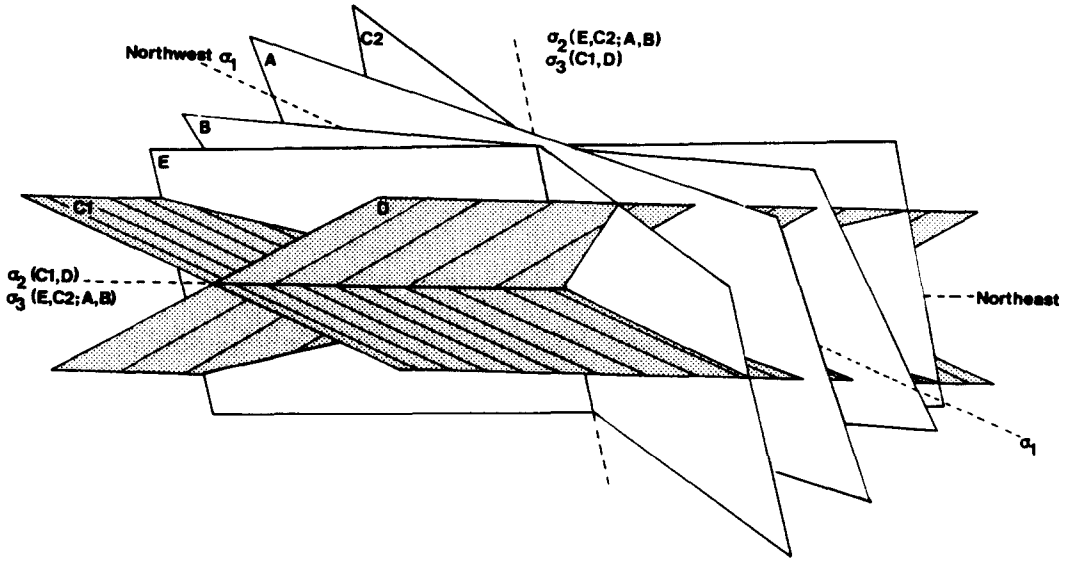

Fig. 11. Stress indicatrix showing stress configuration during three main stages of fracturing.

(c) subvertical to steeply dipping strike–slip conjugate fractures similar to (b), but with decreasing dihedral angle, indicating a decreasing confining pressure in the grid area with time (sets A and B).

(4) The development of the 3-D fracture framework over time illustrates that epidote filled mainly the early subhorizontal to moderately dipping fracture zones, but also was deposited to a minor degree in the incipient steeply dipping fracture zones. These were gradually intensified by the change in stress directions during the second and third stages of fracturing, which deposited mainly chlorite. Subsequent rejuvenation of these fracture zones is demonstrated by the presence of later low-temperature minerals.

(5) Thus the main framework of fractures, filled with epidote and chlorite, was constructed in response to stresses that operated soon after pluton emplacement. Stress changes since then have been relatively minor and have apparently rejuvenated old fracture zones rather than creating new ones. Therefore any investigation of potential waste-disposal sites at depth in similar granitic bodies must consider the early fracture framework as the most likely pathway for movement of toxic solutions between the disposal area and the biosphere.

Acknowledgements—We are grateful to A. Brown and D. Stone for their constructive criticism. I. Ermanovics, G. McCrank and P. Brown also reviewed the manuscript.

REFERENCES

Bailey, A. I. 1975. A method of analyzing polymodal distributions in orientation data. *Math. Geol.* **7**, 285–293.

Bau, A. F. S. 1976. History of regional deformation in the Kashabowie–Lac des Mille Lacs areas northwestern Ontario: progress report. *Proc. 1976 Geotraverse Conference*, Dept. of Geology, University of Toronto, Paper 22, 8.

Brown, P. A., Kamineni, D. C., Stone, D. & Thivierge, R. H. 1980. General geology of the Eye–Dashwa Lakes pluton, Atikokan northwestern Ontario. Current Research, Part A; *Geol. Surv. Pap. Can.*, **80-1A**, 379–384.

Brown, P. A. & McEwen, J. H. 1982. Plutons as hosts? *Geos* **11** (4), 12–15.

Burnham, C. W. & Ohmoto, H. 1980. Late stage processes of felsic magmatism. *Min. Geol.* **8**, 1–11.

Dugal, J. J. B., Hillary, E. M., Kamineni, D. C., Simandl, G. J. & Sikorsky, R. I. 1981. Drilling and core logging programs at the Atikokan research area. AECL Technical Record 174. (Unpublished; available from Atomic Energy of Canada Research Company, Chalk River, Ont. K0J 1J0.)

Fenwick, W. G. 1976. Geology of the Finlayson Lake area, District of Rainy River. Ont. Div. Mines, Geoscience Report 145.

Hibbard, M. J. 1980. Indigenous source of late-stage dikes and veins in granitic plutons. *Econ. Geol.* **75**, 410–423.

Hillary, E. 1982. Geometric representation of subsurface fracturing in boreholes ATK-1, ATK-2, ATK-3, ATK-4 and ATK-5, Atikokan, Northwestern Ontario. AECL Technial Record 182. (Unpublished; available from Atomic Energy of Canada Research Company, Chalk River, Ont. K0J 1J0.)

Hobbs, B. E., Means, W. D. & Williams, P. F. 1976. *An Outline of Structural Geology*. Wiley, Toronto.

Kamb, W. R. 1959. Ice petrofabric observations from Blue Glacier, Washington, in relation to theory and experiment. *J. geophys. Res.* **64**, 1891–1909.

Kamineni, D. C., in press. Sulphur isotope geochemistry of fracture-filling gypsum in an Archean granite near Atikokan, Ontario, Canada. *Chem. Geol.*

Kamineni, D. C. & Dugal, J. J. B. 1982. A study of rock alteration in the Eye–Dashwa Lakes pluton, Atikokan, Northwestern Ontario, Canada. *Chem. Geol.* **36**, 35–57.

Kamineni, D. C. & Stone, D. in press. The ages of fractures in the Eye–Dashwa pluton, Atikokan, Canada. *Contr. Min. Petrol.*

Knapp, R. B. & Norton, D. 1981. Preliminary numerical analysis of processes related to magma crystallisation and stress evolution in cooling pluton environments. *Am. J. Sci.* **281**, 35–68.

McFadden, P. L. 1980. The best estimate of Fisher's precision parameter K. *Geophys. J. R. astr. Soc.* **60**, 397–407.

McFadden, P. L. & Lowes, F. J. 1981. The discrimination of mean directions drawn from Fisher distribution. *Geophys. J. R. astr. Soc.* **67**, 19–33.

Nie, N. W., Hull, C. H., Jenkins, J. G., Steinbrenner, K. & Bent, D. H. 1975. *Statistical Package for the Social Sciences*. McGraw-Hill, New York.

Ramsden, J. & Cruden, D. M. 1979. Estimating densities in contoured orientation diagrams. *Bull. geol. Soc. Am.* **90**, 580–607.

Reches, Z. 1978. Analysis of faulting in three dimensional strain field. *Tectonophysics* **47**, 109–129.

Schwerdtner, W. M., Stone, D., Osadetz, K., Morgan, J. & Stott, G. M. 1979. Granitoid complexes and the Achean tectonic record in the southern part of northwestern Ontario. *Can. J. Earth Sci.* **16**, 1965–1977.

Segall, P. & Pollard, D. D. 1983. Nucleation and growth of strike slip faults in granite. *J. geophys. Res.* **88** (B1), 555–568.

Stauffer, M. R. 1966. An empirical–statistical study of three-dimensional fabric diagrams as used in structural analysis. *Can. J. Earth Sci.* **3**, 473–498.

Stone, D. 1980. Distribution of near vertical surface fractures in the Dashwa pluton, Atikokan, Ontario. AECL Technical Record 125. (Unpublished; available from Atomic Energy of Canada Research Company, Chalk River, Ont. K0J 1J0.)

Stone, D. 1981. Recent geotechnical work at the Atikokan, Ontario research site. In: Proc. Eleventh Information Meeting of the Nuclear Fuel Waste Management Program, Atomic Energy of Canada Limited, Technical Record 180 (Unpublished; available from Atomic Energy of Canada Research Company, Chalk River, Ont. K0J 1J0.)

Stone, D. & Kamineni, D. C. 1982. Fractures and fracture infillings of the Eye–Dashwa Lakes pluton, Atikokan, Ontario. *Can. J. Earth Sci.* **19**, 789–803.

Terzaghi, R. D. 1965. Sources of error in joint surveys. *Geotechnique* **15**, 287–304.